

Emergent Quantum Valley Hall Insulator from Electron Interactions in Transition-Metal Dichalcogenide Heterobilayers

Palash Saha¹ and Michał Żegrodnik^{1,*}

¹*Academic Centre for Materials and Nanotechnology,
AGH University of Krakow, Al. Mickiewicza 30, 30-059 Krakow, Poland*

(Dated: December 3, 2025)

We explore the emergence of topological phases in moiré MoTe₂/WSe₂ bilayer, highlighting the crucial role of spin-orbit coupling and Coulomb interactions at two holes per moiré unit cell $\nu = 2$. Our analysis uncovers robust Quantum Valley Hall Insulating (QVHI) phase and reveals that long-range interactions alone can mediate the interlayer electron tunneling, generating topologically nontrivial bands even in the absence of the corresponding single-particle hopping. Additionally, we show that in the case of band mixing terms originating both from the interaction and single particle physics a competition between topological states realizing *s-wave* and *p ± ip-wave* symmetries can appear. Moreover, within the considered theoretical framework, we present that by introducing a small Zeeman field, one can lift the band inversion in one of the valleys. This leads to a Quantum Anomalous Hall Insulating (QAH) state with the topological gap opening in a single valley and the other being topologically trivial.

I. INTRODUCTION

The exploration of topologically nontrivial and exotic states in moiré superlattices has recently become a key objective in condensed matter physics. In particular, transition metal dichalcogenide (TMD) bilayers due to lattice mismatch or rotational misalignment have lead to experimental observation of topologically protected edge states [1–3], unconventional superconductivity [4, 5], correlated insulating states [6–8] as well as generalized Wigner crystals [9, 10]. Due to the presence of narrow electronic bands, it is believed that effects related with electron-electron interactions may play a significant role in the emergence of the variety of observed physical phenomena.

One of the characteristic features of the TMD-based bilayer systems is the presence of strong Ising-type spin-orbit coupling, which leads to spin-valley locking [11–13]. In the AB stacked MoTe₂/WSe₂ heterobilayer, a nonzero band offset separates the spin-valley locked bands originating from the upper and lower layer, leading to a band insulator at two holes per moiré unit cell $\nu = 2$. By applying a perpendicular electric field, one can significantly reduce the band gap, enabling the band inversion necessary for a topological phase transition [14, 15]. Such physical picture is consistent with the experimentally observed Quantum anomalous Valley Hall behavior (QVHI) [16, 17]. Furthermore, at one hole per moiré unit cell $\nu = 1$ (half-filling of the upper band), instead of a band insulator a Mott (or charge transfer) insulator emerges, which is due to the strong Coulomb repulsion. In this case, after the application of the displacement field a transition to a Quantum Anomalous Hall Insulator (QAH) is observed [16].

First-principles calculations and the continuum model

approach have been utilized to search for QVHI phases in MoTe₂/WSe₂ heterobilayer [14, 18]. Also, interaction driven quantum valley Hall effects have been studied in the continuum limit using plane wave basis [19] and pseudomagnetic fields [20]. The role of electron-electron interactions has also been emphasized in the analysis topological bands of the QAH state [18, 21–25] as well as heavy-fermion/Kondo [26, 27] and excitonic [28, 29] physics. These analysis suggest that single-particle physics alone is insufficient to capture the low-energy behavior of the MoTe₂/WSe₂ system.

Our work is motivated by the experimental findings [16, 17] that demonstrate a continuous topological phase transition from a moiré band insulator to a QVHI at two holes per moiré unit cell in the AB-stacked MoTe₂/WSe₂ heterobilayer. It should be noted that in the lowest order continuum model of this system, the interlayer spin-flip hopping which is necessary to induce the topological features is vanishingly small. Here, we apply a minimal model composed of two moiré valence bands, supplemented by intra- and inter-site Coulomb repulsion terms treated with the use of Hartree-Fock method (HF). We show that Coulomb interaction-assisted interlayer hopping can effectively replicate the crucial spin-flip tunneling, leading to a non-trivial band topology consistent with QVHI state. We calculate the winding number of this topological gap's complex phase in the neighborhood of nodal points which determine the topological features of the model. Moreover, in the presence of both interaction induced band mixing and small single particle mixing term a competition between two topological states realizing different symmetries can appear. Additionally, we show that within the presented theoretical framework one can lift the spin-valley degeneracy in the \mathcal{T} invariant QVHI [30] state by using the Zeeman field as discussed in the recent experimental report [17]. In such a case, the band inversion and emergence of topological bands become confined to one valley, leaving the other topologically trivial. Ultimately, this presents a route to

* michal.zegrodnik@agh.edu.pl

realize \mathcal{T} symmetry broken QAHI from QVHI at $v = 2$ via the interplay between the external magnetic field and electron-electron interaction effects. Note that although an external magnetic field is applied, it does not result in a conventional Quantum Hall effect due to absence of Landau level formation [31].

The paper is structured as follows: In Sec. II, we introduce the extended Hubbard model and outline the implementation of the HF approach. Sec. III explores in detail the topological properties of the considered system as induced by the interlayer interaction term. In the second part of Sec. II, we study the influence of Zeeman field in bridging the QVHI and QAHI phase. Finally, in Section. IV we summarize and conclude the important results.

II. MODEL AND METHOD

As shown in Ref. [14], the minimal model of the AB-stacked MoTe₂/WSe₂ can be composed of two moiré Wannier orbitals centered at the XX ($X = \text{Te, Se}$) and MM ($M = \text{Mo, W}$) stacking points in the WSe₂ and MoTe₂ layers, respectively. In order to take into account electron-electron interactions we supplement the model with both onsite and intersite Coulomb repulsion terms, which results in the extended Kane-Mele-Hubbard Hamiltonian of the form

$$\hat{\mathcal{H}} = \hat{\mathcal{H}}_t + \hat{\mathcal{H}}_{UV} + \hat{\mathcal{H}}_B, \quad (1)$$

where the first term represents the single-particle part, shown explicitly below

$$\begin{aligned} \hat{\mathcal{H}}_t = & \sum_{\langle\langle ij \rangle\rangle l \sigma} t_{ij\sigma}^l \hat{c}_{il\sigma}^\dagger \hat{c}_{jl'\sigma} + \sum_{\langle ij \rangle \sigma} (t_{ij\sigma\bar{\sigma}}^{12} \hat{c}_{i1\sigma}^\dagger \hat{c}_{j2\bar{\sigma}} + H.c.) \\ & + (D + \Delta) \sum_i \hat{n}_{il=2}, \end{aligned} \quad (2)$$

with $\hat{c}_{il\sigma}^\dagger$ ($\hat{c}_{il\sigma}$) being the creation (annihilation) operator for an electron of spin σ in the Wannier orbital at site i and $\langle\langle ij \rangle\rangle$ denotes next-nearest-neighbor (NNN) pairs on the honeycomb lattice (intralayer hoppings) while $\langle ij \rangle$ denotes nearest-neighbor (NN) pairs (interlayer hoppings). Above, we introduced a layer index l to distinguish between MM ($l = 1$) and XX ($l = 2$) orbitals corresponding to two triangular sublattices, which together form a honeycomb structure. It should be noted that high values of spin-orbit interaction in TMDs lead to a strong coupling between spin and valley degrees of freedom, effectively locking them together. When MoTe₂ and WSe₂ are stacked in an AB configuration, the spin-valley locking exhibits an opposite orientation in the two layers. In the minimal picture considered here, this leads to complex hoppings of the following form

$$t_{ij\sigma}^{ll} = t_l e^{i\phi_{\parallel}\sigma^z\nu_{ij}} \quad (3)$$

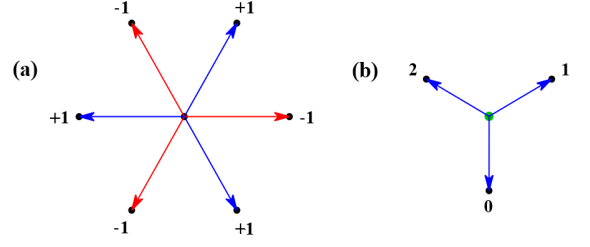


FIG. 1. (a) The direction dependent sign parameter $\nu_{ij} = \pm 1$ for the six NNN hoppings appearing in Eq. (3), (b) The $\eta_{ij} = 0, 1, 2$ parameters for the three NN hoppings appearing in Eq. 4.

$$t_{ij\sigma\bar{\sigma}}^{12} = t_{\perp} e^{i\phi_{\perp}\sigma^z\eta_{ij}}, \quad (4)$$

where, the spin index is given by $\sigma^z = 1(-1)$ for $\sigma = \uparrow(\downarrow)$, respectively. The parameter $\nu_{ij} = \pm 1$ is determined by the intralayer hopping direction (cf. Fig. 1) while $\eta_{ij} = 0, 1, 2$ enumerates different interlayer hopping directions, increasing counterclockwise around the WSe₂ lattice sites. Finally, the complex phases of the hoppings are $\phi_{\parallel} = \phi_{\perp} = 2\pi/3$. However, for the sake of completeness, in the following we also consider the case of $\phi_{\parallel} = 2\pi/3$ and $\phi_{\perp} = 0$. The structure of the single-particle part of the Hamiltonian is analogical to that of the Kane-Mele model, however, in the latter one typically takes $\phi_{\parallel} = \pi/2$ and $\phi_{\perp} = 0$. The hopping amplitudes are adopted from Ref. 14 and have the values $t_1 = 4.03$ meV and $t_2 = 3.4$ meV. As discussed in Appendix A, the rise of spin-flip hybridization leads to an immediate effect contributing to the loss of flavor symmetry and spin valley locking.

The third term in Eq. (2) represents the onsite contribution, where the particle number operator is defined as $\hat{n}_{il} = \hat{n}_{il\uparrow} + \hat{n}_{il\downarrow}$ with $\hat{n}_{il\sigma} = \hat{c}_{il\sigma}^\dagger \hat{c}_{il\sigma}$. Here, $\Delta = -60$ meV characterizes an intrinsic band offset, while D accounts for the influence of the displacement field. When $D = 0$, the top and bottom bands are primarily formed by MoTe₂ and WSe₂ states, respectively, with a band gap between them. As D increases, the bottom band shifts upward, eventually leading to band inversion[14].

The second term of Hamiltonian (1) corresponds to electron-electron interactions and has the form

$$\hat{\mathcal{H}}_{UV} = U \sum_{il} \hat{n}_{il\uparrow} \hat{n}_{il\downarrow} + V \sum'_{ijll'\sigma} \hat{n}_{il} \hat{n}_{jl'}, \quad (5)$$

where U and V correspond to onsite and intersite Coulomb repulsion integrals and the primed summation means NN neighbor contributions are taken in account.

As a part of our analysis we aim at studying the influence of external magnetic field on the topological properties of the system. Therefore, we supplement our model with a Zeeman term of the form

$$\hat{\mathcal{H}}_B = \mu_B g \sum_{\mathbf{k}} \mathbf{B} \cdot \hat{\mathbf{S}}(\mathbf{k}), \quad (6)$$

where μ_B is the Bohr magneton, g is the Landé g-Factor and

$$\hat{\mathbf{S}}(\mathbf{k}) = \frac{1}{2} \sum_{\mathbf{k}\alpha\beta} \hat{c}_{\mathbf{k}\alpha}^\dagger \sigma_{\alpha\beta} \hat{c}_{\mathbf{k}\beta}, \quad (7)$$

is the spin operator with σ being the Pauli matrices and $\alpha, \beta = [\uparrow, \downarrow]$. We focus on the typical situation of out of plane \mathbf{B} with zero inplane magnetic field terms.

After applying the Hartree-Fock (HF) approximation to the interaction part of the model, we obtain

$$\begin{aligned} \hat{\mathcal{H}}_{UV} \approx & U \sum_{il} (\langle \hat{n}_{il\uparrow} \rangle \hat{n}_{il\downarrow} + \hat{n}_{il\uparrow} \langle \hat{n}_{il\downarrow} \rangle - \langle \hat{n}_{il\uparrow} \hat{n}_{il\downarrow} \rangle) \\ & + \frac{1}{2} V \sum'_{ijll'\sigma} (\langle \hat{n}_{il\sigma} \rangle \hat{n}_{jl'\sigma'} + \hat{n}_{il\sigma} \langle \hat{n}_{jl'\sigma'} \rangle - \langle \hat{n}_{il\sigma} \hat{n}_{jl'\sigma'} \rangle \\ & - (\mathcal{P}_{i\sigma j\bar{\sigma}}^{ll'})^* \hat{\mathcal{P}}_{i\sigma j\bar{\sigma}}^{ll'} - \mathcal{P}_{i\sigma j\bar{\sigma}}^{ll'} \hat{\mathcal{P}}_{j\bar{\sigma} i\sigma}^{l'l} + \mathcal{P}_{i\sigma j\bar{\sigma}}^{ll'} (\mathcal{P}_{i\sigma j\bar{\sigma}}^{l'l})^*), \end{aligned} \quad (8)$$

where $\hat{\mathcal{P}}_{i\sigma j\bar{\sigma}}^{ll'} = \hat{c}_{il\sigma}^\dagger \hat{c}_{jl'\bar{\sigma}}$ and $\mathcal{P}_{i\sigma j\bar{\sigma}}^{ll'} = \langle \hat{c}_{il\sigma}^\dagger \hat{c}_{jl'\bar{\sigma}} \rangle$.

In the next step, we rewrite our Hamiltonian in a compact form after the transformation to \mathbf{k} -space. Namely,

$$\begin{aligned} \hat{H} = & \sum_{\mathbf{k}\sigma} \hat{\mathbf{f}}_{\mathbf{k}\sigma}^\dagger \mathbf{H}_{\mathbf{k}\sigma} \hat{\mathbf{f}}_{\mathbf{k}\sigma} + U \sum_{il} \langle \hat{n}_{il\uparrow} \hat{n}_{il\downarrow} \rangle \\ & - \frac{V}{2} \left(\sum_{ij\sigma\sigma'} \langle \hat{n}_{i1\sigma} \hat{n}_{j2\sigma'} \rangle - \sum_{ij\sigma} \mathcal{P}_{i\sigma j\bar{\sigma}}^{12} \mathcal{P}_{j\bar{\sigma} i\sigma}^{21} \right), \end{aligned} \quad (9)$$

where we kept the trivial non-operator terms in the real space representation while $\hat{\mathbf{f}}_{\mathbf{k}\sigma}^\dagger = (\hat{c}_{\mathbf{k}1\sigma}^\dagger, \hat{c}_{\mathbf{k}2\bar{\sigma}}^\dagger)$ and $\hat{\mathbf{f}}_{\mathbf{k}\sigma} = (\hat{\mathbf{f}}_{\mathbf{k}\sigma}^\dagger)^\dagger$ are composite creation and annihilation operators in \mathbf{k} -space and

$$\mathbf{H}_{\mathbf{k}\sigma} = \begin{pmatrix} \varepsilon_{\mathbf{k}\sigma}^{11} & \varepsilon_{\mathbf{k}\sigma}^{12} \\ \varepsilon_{\mathbf{k}\sigma}^{21} & \varepsilon_{\mathbf{k}\sigma}^{22} \end{pmatrix}. \quad (10)$$

The explicit form of the Hamiltonian matrix elements have the following form

$$\varepsilon_{\mathbf{k}\sigma}^{11} = \sum_{\langle\langle i(j) \rangle\rangle} t_{ij\sigma}^{11} e^{i\mathbf{k}(\mathbf{R}_{i1} - \mathbf{R}_{j1})} + U \langle \hat{n}_{kl\bar{\sigma}} \rangle + 3V \langle \hat{n}_{k2} \rangle, \quad (11)$$

$$\varepsilon_{\mathbf{k}\sigma}^{22} = \sum_{\langle\langle i(j) \rangle\rangle} t_{ij\bar{\sigma}}^{22} e^{i\mathbf{k}(\mathbf{R}_{i2} - \mathbf{R}_{j2})} + U \langle \hat{n}_{k2\sigma} \rangle + 3V \langle \hat{n}_{k1} \rangle + D + \Delta, \quad (12)$$

$$\varepsilon_{\mathbf{k}\sigma}^{l\bar{l}} = \sum_{\langle\langle i(j) \rangle\rangle} (t_{ij\sigma\bar{\sigma}}^{l\bar{l}} - V \mathcal{P}_{j\sigma i\bar{\sigma}}^{l\bar{l}}) e^{i\mathbf{k}(\mathbf{R}_{il} - \mathbf{R}_{j\bar{l}})}, \quad (13)$$

where \mathbf{R}_{il} vector corresponds to lattice site i on the sublattice l . It should be noted that within the mean-field picture the V -term can lead to two effects. One of them corresponds to the onsite energy contribution, which effectively shifts the bands and as a result modifies the energy gap between them [cf. Eqs. (11) and (12)]. This

acts like an additional displacement field tuned by V . In addition, a contribution to the NN hopping terms appears with an effective amplitude equal to $V \mathcal{P}_{i\sigma j\bar{\sigma}}^{l'l}$ [cf. Eq. (13)]. Due to the specifics of the considered band structure, the spin-conserving HF contribution of the density-density Coulomb interaction term cannot be operative and therefore is not taken in account.

In our previous work [23] we considered the case of one hole per moiré unit cell which leads to a half-filled upper band. In such situation the onsite Coulomb term leads to antiferromagnetism which comes with the cost of losing spin rotational invariance and splitting of the upper band into two sub-bands. Therefore, an antiferromagnetic charge transfer insulating state is realized which after band inversion generates QAHI state. In contrast, the present study corresponds to two holes per moiré unit cell meaning that a fully filled lower band and fully empty upper band appears. Now the spin degrees of freedom cannot easily establish a magnetically ordered arrangement with neighboring sites. Therefore, we do not consider any spin-ordering here.

A key aspect of the considered system is that the spin-up valley in MoTe₂ is located at the opposite K -point of the monolayer Brillouin zone with respect to the spin-up valley in WSe₂ as in Ref.[14]. Therefore, after the band inversion induced by the displacement field, a topological gap can only be opened by interlayer terms, which couple distinct valleys. Due to spin-valley locking these terms are of spin-flip character. For the sake of generality, our model contains such terms already in the single-particle part of the Hamiltonian. However, as already mentioned according to lowest order continuum modeling, the spin-flip hopping amplitudes would be vanishingly small [18]. Therefore, here we propose that long-range interactions alone can mediate an effective interlayer hopping mechanism coupling orbitals from different layers and eventually giving rise to topologically nontrivial bands even when the hybridization term is absent in the single-particle Hamiltonian. As can be seen from Eqs. (11) and (12) such mechanism can already appear at the mean-field level. However, for the case of $t_\perp = 0$, this would require spontaneous symmetry breaking leading to a situation in which $\mathcal{P}_{i\sigma j\bar{\sigma}}^{l'l} \neq 0$ (for $l \neq l'$) results purely due to interactions. In such a case the Coulomb repulsion together with the specific type of spin-valley locking would lead to an emergent topological state. The analysis of such a scenario is the starting point of the current work.

III. RESULTS

Our analysis focuses on the extended Kane-Mele-Hubbard model applied to the AB-stacked MoTe₂/WSe₂ heterobilayer. We employ a self-consistent HF mean-field approach at the integer filling of two holes per moiré unit cell $\nu = 2$, for which experiments have revealed a continuous topological phase transition from a moiré band in-

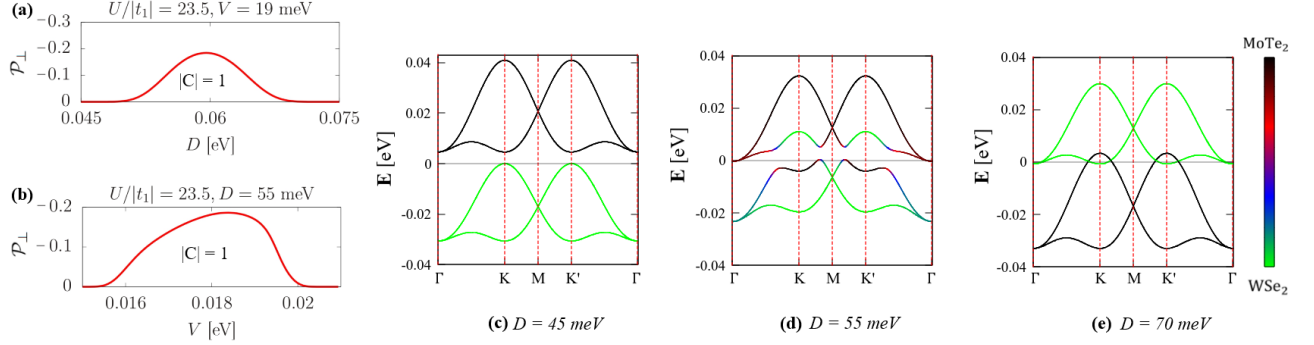


FIG. 2. (a),(b) The interlayer tunneling expectation value \mathcal{P}_\perp as a function of the displacement field and Coulomb interaction for the special case of $t_\perp = 0$. The band structures in (c), (d), and (e) correspond to the band insulator phase, the QVHI phase, and to the metallic behavior and have been obtained for displacement field values $D = 45$ meV, $D = 55$ meV, and $D = 70$ meV, respectively with the interaction strengths fixed at $V = 19$ meV. The results have been obtained for $U = 94.7$ meV and $n = 2$, which is equivalent to two holes per moiré unit cell.

insulator to a Quantum Valley Hall Insulator. Within our two-band picture the experimental situation of $v = 2$ corresponds to the lower band being completely filled and the upper band being empty. In the following, we use the electron language in which the number of electrons per moiré unit cell is $n = 4 - v$, meaning that $v = 2$ corresponds to $n = 2$.

A. QVHI state formation

First, we analyze the possibility of creating a topological state purely via Coulomb-assisted spin-flip hopping when $t_\perp = 0$ and $\mathbf{B} = 0$. As seen from Eq. (11) and (12) this requires $|\mathcal{P}_{ij\sigma}^{ll'}| \neq 0$ for $l \neq l'$, possibly leading to the creation of topological states characteristic for the QVHI. In Figs. 2 (a) and (b) we show that in a certain range of model parameters, such a QVHI state can become stable. In the obtained solution the following rule takes place: $|\mathcal{P}_{ij\sigma}^{ll'}| = \mathcal{P}_\perp \in \mathbb{R}$ for $l \neq l'$ for all six possible NN pairs. Therefore, the mixing term induced by the Coulomb interactions does not fully resemble the one that appeared in the original single-particle Hamiltonian [cf. Eq. (4)]. Nevertheless, it still leads to non-trivial topological features; hence, the non-zero values of \mathcal{P}_\perp lead to opening of a topological gap, and the Chern number being $C = 1$ and $C = -1$ corresponding to the two valleys K and K' , respectively. Due to purely real NN hopping amplitudes in all directions, the resulting topological gap corresponds to the A_1 irreducible representation (s -wave symmetry).

As one can see in Fig. 2 (b), to induce $\mathcal{P}_\perp \neq 0$ it is necessary to have significant Coulomb repulsion since the effective spin-flip term is proportional to V . However, as can be deduced from Eqs. (11) and (12), too large values of V increase the energy gap between the bands originating from the two layers. This can make the interlayer

mixing term not operative, leading to the suppression of \mathcal{P}_\perp and consequently to the destruction of the topological state. Additionally, since the displacement field also tunes the gap between the bands, it has to be in proper range so that the interlayer mixing is possible as visible in Fig 2(a). Initially, by increasing D one moves the bands closer to each other which works in favor of generating nonzero values of \mathcal{P}_\perp . However, too large values of D lead to the WSe₂ band being placed above the band originating from the MoTe₂ layer. In such a regime, further increase of D enhances the band gap which has a negative influence on the mixing and suppresses \mathcal{P}_\perp .

To better understand the sequence of phases shown in Fig. 2 we present the band structure for three representative values of the gate voltage values ($D = 45$ meV, $D = 55$ meV, $D = 70$ meV) each corresponding to Coulomb interaction $V = 19$ meV and $U = 94.7$ meV. With increasing D one encounters a following phases: (i) moiré band insulator with the MoTe₂ and WSe₂ bands being separated by a significant band gap with $\mathcal{P}_\perp = 0$; (ii) QVHI state where the band inversion appears together with $\mathcal{P}_\perp \neq 0$ leading non-trivial topology; (iii) metallic state in which the spin-flip terms are again suppressed to zero. Note, that the continuous phase transition from band insulator to QVHI obtained by us here is consistent with the key experimental results shown in Refs. [16, 17].

B. Symmetry of the topological state

In Fig. 3(a), we provide the calculated interlayer spin-flip expectation value \mathcal{P}_\perp which leads to topological gap opening in certain region of the (D, V) -plane. This region corresponds to QVHI state with $C = \pm 1$. As one can see, $V_{\text{opt}} \approx 18 - 19$ meV corresponds to relatively large topological gap and the appearance of the QVHI state, which remains stable within a displacement field

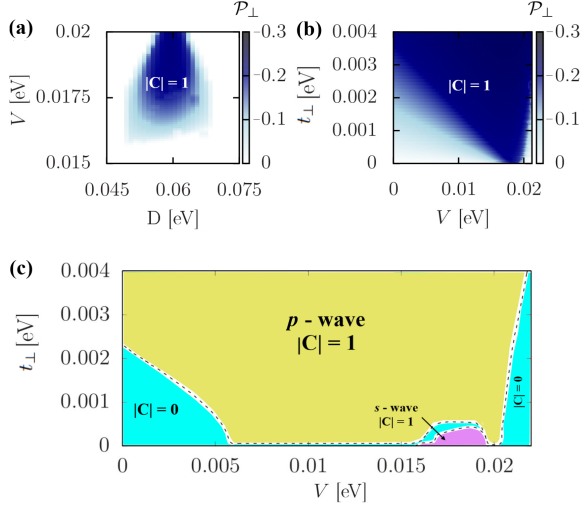


FIG. 3. (a) The interlayer tunneling expectation value \mathcal{P}_\perp as function of the displacement field (D) and intersite Coulomb interaction (V) for $t_\perp = 0$. (b) The interlayer tunneling expectation value \mathcal{P}_\perp as function of V and t_\perp for selected displacement field $D = 55$ meV and $\phi_\perp = 0$. (c) The phase diagram of the model at the (t_\perp, V) -plane for $D = 55$ meV and $\phi_\perp = 2\pi/3$. The two topological states seen in (c) correspond to a $p \pm ip$ and s -wave symmetries of the gap.

window between approximately 50 meV and 70 meV. It should be noted that the determined optimal value of V is comparable to the width of the single band of the model ($W \approx 20 - 30$ meV). Additionally, in Fig. 3 (b) and (c) we consider a situation in which the interaction induced NN hopping is supplemented with a contribution resulting from the single-particle part of our Hamiltonian. For purely real single-particle hopping amplitude ($t_\perp \neq 0$ and $\phi_\perp = 0$) the effect is rather trivial. Namely, increasing t_\perp stabilizes the topological phase, making it more robust in the diagram. In such case, even for $V = 0$ one can induce the $|C| \neq 0$ situation.

An interesting situation takes place when the contribution to the NN hopping originating from the single-particle terms is characterized by a complex amplitude with $\phi_\perp = 2\pi/3$ [cf. Eq. (4)]. Such particular phase appearing in the single particle part of the Hamiltonian has been considered in Ref. [14]. As one can see from Fig. 3 (c), in such a case a competition between two topological states appears. The first is characterized by an s -wave symmetry of the topological gap, while in the second a $p \pm ip$ symmetry is realized. The s -wave state is promoted by the interaction-based mechanism analyzed earlier and appears in a relatively narrow window of V and very small t_\perp amplitude. As t_\perp increases, the tendency towards the $p \pm ip$ symmetry arises and at some point the NN tunneling expectation values ($\mathcal{P}_{i\sigma j\bar{\sigma}}^{ll'}$ for $l \neq l'$) start to reproduce the complex phase pattern originating from the single particle term. However, there is a narrow transition region in which $|C| = 0$.

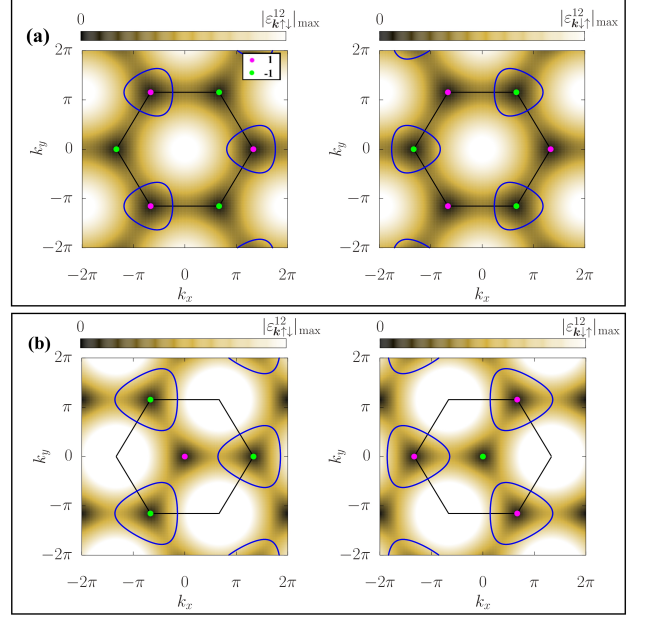


FIG. 4. Absolute value of the topological gap ($|\epsilon_{\mathbf{k}\sigma\bar{\sigma}}^{12}|$) as a function of momentum for pure s -wave (a) and $p \pm ip$ -wave (b) symmetries. The magenta and green dots mark the positions of the Chern charges of the value 1 and -1 , respectively. (a) and (b) correspond to $t_\perp = 0$ and $t_\perp = 3$ meV with $\phi_\perp = 2\pi/3$. The remaining model parameters are $V = 19$ meV, $D = 55$ meV and $U = 94.7$ meV.

To gain more insight when it comes to the differences between the two obtained topological states, in Fig. 4 we provide the color maps showing the absolute value of the \mathbf{k} -dependent topological gaps, $|\epsilon_{\mathbf{k}\sigma\bar{\sigma}}^{12}|$. Note, that the gap opening is caused by the anti-diagonal terms appearing in the matrix form of our Hamiltonian [cf. Eq. (10)]. One of the visible differences is that in the s -wave scenario the absolute value of the gap is C_6 symmetric and does not depend on the spin configuration, while in the p -wave case a two $2\pi/3$ rotated patterns are created corresponding to the two spin configurations, which are C_3 symmetric each. In both situations, nodal points appear at the K and K' points for which $|\epsilon_{\mathbf{k}\sigma\bar{\sigma}}^{12}| = 0$. However, for the $p \pm ip$ symmetry, there is an additional nodal point at Γ . Note that each nodal point introduces a topological charge and the Chern number can be calculated by using the following formula

$$C = \sum_{i \in \Omega_F} (-1)^w C_i, \quad (14)$$

where C_i is the topological charge of a given nodal point which can be determined by calculating the winding of the complex phase of $\epsilon_{\mathbf{k}\sigma\bar{\sigma}}^{12}$ around it with $w = 0$ (1) for the clockwise (anticlockwise) direction. It is important to note that index i in the summation above runs over the nodal points contained inside the closed curve determined by the condition $\epsilon_{\mathbf{k}\sigma}^{11} = \epsilon_{\mathbf{k}\sigma}^{22}$ (cf. Appendix B). Both the values of the nodal points and the C_F curves are

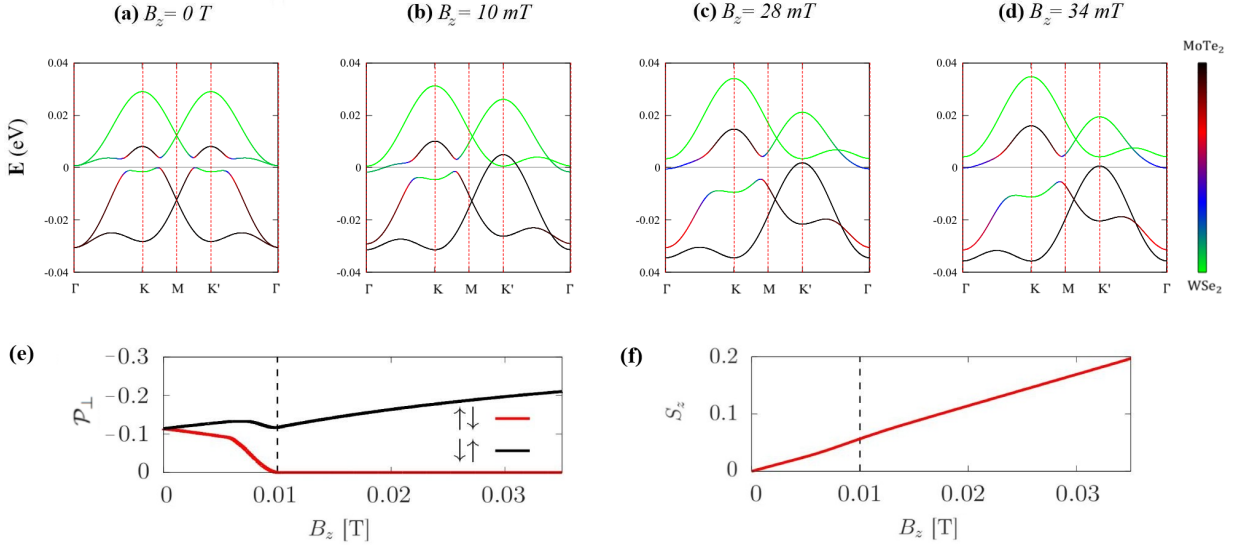


FIG. 5. (a-d) Band structure along high symmetry directions for selected values of the Zeeman field provided in the figures and for $D = 73$ meV, $U = 129$ meV, $V = 24$ meV. In (e) and (f) we show the B_z -dependence of interlayer mixing expectation values $|\mathcal{P}_{i\uparrow j\downarrow}^{12}| \equiv \mathcal{P}_{\perp}^{\uparrow\downarrow}$ and $|\mathcal{P}_{i\downarrow j\uparrow}^{12}| \equiv \mathcal{P}_{\perp}^{\downarrow\uparrow}$ as well as the spin magnetization S_z .

provided in Fig. 4. It can be clearly seen that both scenarios lead to the Chern number $|C| = 1$ for each valley. Due to spin-valley locking the two valleys are characterized by opposite Chern numbers which leads to QVHI state. Note that the topological charge of each K and K' point has to be divided by 3 since it is shared by three Brillouin zones. The values of the Chern numbers has been additionally calculated by using the Brillouin zone triangulation method which gives the same results as the procedure described above.

C. Influence of Magnetic Field

Following the recent experimental report [17] we try to replicate the proposed topological phase transition induced by the presence of external magnetic field within the Coulomb-assisted hopping scenario presented by us in the previous Section (for $t_{\perp} = 0$). Within the considered model, the Zeeman term can tune the topological gaps appearing at the two valleys of the mini Brillouin zone. However, with increasing B_z , the gap in one valley is enhanced while the other is suppressed.

We start with the following model parameters $U = 129$ meV, $V = 24$ meV, and $D = 73$ meV which lead to a topological gap opened as shown in Fig. 5(a) for $B_z = 0$. Similarly as before in such a situation we have $\mathcal{P}_{i\sigma j\bar{\sigma}}^{ll'} \equiv \mathcal{P}_{\perp} \neq 0$. However, under the application of small nonzero B_z the band inversion is reduced in the K' valley, and consequently $|\mathcal{P}_{i\uparrow j\downarrow}^{12}| \equiv \mathcal{P}_{\perp}^{\uparrow\downarrow}$ is significantly suppressed since it corresponds to band mixing in the same valley [cf. Fig. 5(d)]. At the same time, the opposite situation takes place in the K valley where the band inversion is enhanced together with the value of $|\mathcal{P}_{i\downarrow j\uparrow}^{12}| \equiv \mathcal{P}_{\perp}^{\downarrow\uparrow}$. For

the critical value of $B_z = 10$ mT some small band inversion at K' still appears but the corresponding Coulomb assistant hopping is already zero. This leads to a loss of topological properties of one-half of the considered Kane-Mele-Hubbard model. Nevertheless, the K -valley gap is still topological. In such a state, a combination of topological insulating and normal metallic behavior appears. Further enhancement of the Zeeman term leads to opening of a trivial band gap at K' and enhancement of the topological gap at K meaning that a QAHI state should be observed [cf. Fig. 5(d)]. As a consequence under the influence of Zeeman effect we have a transition from QVHI state to QAHI state under fixed bias and interaction strengths (both on-site and inter-site).

IV. CONCLUSIONS

In summary, we carry out a detailed theoretical investigation of AB-stacked $\text{MoTe}_2/\text{WSe}_2$ heterostructure at $\nu = 2$ and propose that the non-trivial topology in this structure can be driven by many body interactions. Our analysis is motivated by the lowest order continuum modeling due to which the spin-flip hopping amplitudes in the single particle part of the model, potentially leading to topological state, should be vanishingly small [18]. We show that the Coulomb interaction-assisted interlayer hopping can lead to the opening of an s -wave topological gap leading to a QVHI state even in the absence of the single-particle band mixing term. In order to create favorable conditions for such a spontaneously formed topological state, the NN Coulomb interactions must be relatively strong, with the optimal value being $V_{\text{opt}} = 18$ -19 meV. In such a situation, by increas-

ing the displacement field one encounters the following sequence of phases: (i) moiré band insulator; (ii) QVHI state (iii) metallic state. The continuous phase transition from band insulator to QVHI obtained here is consistent with the key experimental results shown in Refs. [16, 17].

For the sake of completeness we also consider a situation in which the band mixing term originates both from the interaction induced mechanism and due to the single-particle physics. In such a case, competition between *s*-wave and *p*±*ip*-wave topological states appears when the single particle term is additionally characterized by a complex hopping phase $\phi_\perp = 2\pi/3$. As we show, the main difference between the two states is that in the *p*±*ip*-wave case the \mathbf{k} -dependent topological gap has an additional Chern charge residing at the Γ point, which is absent for the *s*-wave state. However, since in both situations the Chern charges of the *K* and *K'* points determine the topological features, the two situations lead to QVHI with $C = \pm 1$.

Finally, we show that the topological phase transition induced by the presence of external magnetic field analyzed in experiments[17] can be reproduced within the Coulomb-assisted hopping scenario considered by us. In such a case, the application magnetic field produces trivial gap at one valley with enhancement of topological gap at the other one thereby favoring the realization of a QAH phase.

The data behind the figures are available in the open repository [32].

ACKNOWLEDGMENTS

We acknowledge discussions with Louk Rademaker and Julian Czarnecki. This research was partly supported by National Science Centre, Poland (NCN) according to Decision No. 2021/42/E/ST3/00128. For the purpose of Open Access, the author has applied a CC-BY public copyright licence to any Author Accepted Manuscript (AAM) version arising from this submission.

Appendix A: Flavor Symmetry

It should be noted that before any emergence of hybridization strong Ising spin-orbit coupling locks spin to valley (τ) in each layer (l) making the two degrees of freedom effectively interchangeable. The flavor space of the model is thus created by the $(l \otimes \tau)$ subspace which is appropriate for the low energy physics. Hence we get a 4 dimensional flavor space spanned by $\{(1K), (1K'), (2K), (2K')\}$. Due to lack of inter-flavor coupling, each flavor conserves its own particle number which is why the flavor-space Hamiltonian is invariant under $U(1)_{1K} \times U(1)_{2K} \times U(1)_{1K'} \times U(1)_{2K'}$ symmetry.

If $|t_\perp| \neq 0$ onset of spin-conserving interlayer mixing is still able to conserve separate particle numbers in each

valley but fails to do the same for layer indices lowering the symmetry to $U(1)_{K\sigma} \times U(1)_{K'\bar{\sigma}}$. The special case in which the single particle physics of this heterobilayer is worked out has only finite spin flip hybridization (\mathcal{P}_\perp) thus destroying the spin-valley locked feature but with the same symmetry of $U(1)_K \times U(1)_{K'}$ without the spin indices.

Appendix B: Chern number as a winding number

Here we provide details related with the characterization of the topological features of the considered model based on the winding number. We start with rewriting the matrix form of our Hamiltonian in a compact form

$$\hat{H} = \sum_{\mathbf{k}\sigma} \hat{\mathbf{f}}_{\mathbf{k}\sigma}^\dagger \mathbf{H}_{\mathbf{k}\sigma} \hat{\mathbf{f}}_{\mathbf{k}\sigma} \quad (\text{B1})$$

where $\hat{\mathbf{f}}_{\mathbf{k}\sigma}^\dagger = (\hat{c}_{\mathbf{k}1\sigma}^\dagger, \hat{c}_{\mathbf{k}2\bar{\sigma}}^\dagger)$ and

$$\mathbf{H}_{\mathbf{k}\sigma} = \begin{pmatrix} \varepsilon_{\mathbf{k}\sigma}^{11} & \varepsilon_{\mathbf{k}\sigma}^{12} \\ \varepsilon_{\mathbf{k}\sigma}^{21} & \varepsilon_{\mathbf{k}\sigma}^{22} \end{pmatrix}. \quad (\text{B2})$$

In the above Hamiltonian we have omitted the trivial non-operator terms since they are not important in the context considered here. The eigenvalues of the Hamiltonian matrix are the following

$$\lambda_{\mathbf{k}\sigma}^{(\pm)} = \frac{\varepsilon_{\mathbf{k}\sigma}^{11} + \varepsilon_{\mathbf{k}\sigma}^{22}}{2} \pm \delta_{\mathbf{k}\sigma}, \quad (\text{B3})$$

where

$$\delta_{\mathbf{k}\sigma} = \sqrt{\zeta_{\mathbf{k}\sigma}^2 + |\varepsilon_{\mathbf{k}\sigma}^{12}|^2}, \quad \zeta_{\mathbf{k}\sigma} = \frac{\varepsilon_{\mathbf{k}\sigma}^{11} - \varepsilon_{\mathbf{k}\sigma}^{22}}{2}. \quad (\text{B4})$$

The corresponding eigenvectors can be expressed in the form

$$\begin{aligned} \text{for } \lambda_{\mathbf{k}\sigma}^{(+)} : \quad |u_{\mathbf{k}\sigma}^{(+)}\rangle &= \begin{pmatrix} e^{i\phi_{\mathbf{k}\sigma}} \cos \frac{\theta_{\mathbf{k}\sigma}}{2} \\ \sin \frac{\theta_{\mathbf{k}\sigma}}{2} \end{pmatrix}, \\ \text{for } \lambda_{\mathbf{k}\sigma}^{(-)} : \quad |u_{\mathbf{k}\sigma}^{(-)}\rangle &= \begin{pmatrix} e^{i(\phi_{\mathbf{k}\sigma} - \pi)} \sin \frac{\theta_{\mathbf{k}\sigma}}{2} \\ \cos \frac{\theta_{\mathbf{k}\sigma}}{2} \end{pmatrix}, \end{aligned} \quad (\text{B5})$$

with the parameters $\theta_{\mathbf{k}\sigma}$ and $\phi_{\mathbf{k}\sigma}$ defined as

$$\theta_{\mathbf{k}\sigma} = 2 \tan^{-1} \left(\frac{\delta_{\mathbf{k}\sigma} - \zeta_{\mathbf{k}\sigma}}{|\varepsilon_{\mathbf{k}\sigma}^{12}|^2} \right), \quad \phi_{\mathbf{k}\sigma} = \arg(\varepsilon_{\mathbf{k}\sigma}^{12}), \quad (\text{B6})$$

where

$$\theta_{\mathbf{k}\sigma} \in [0, \pi], \quad \phi_{\mathbf{k}\sigma} \in [0, 2\pi]. \quad (\text{B7})$$

Note, that for a given eigen-state and by using Eqs. (B5) one can map every \mathbf{k} point of the Brillouin zone onto the Bloch sphere with the parameters $\theta_{\mathbf{k}\sigma}$ and $\phi_{\mathbf{k}\sigma}$ interpreted as spherical coordinates and $|2\sigma\rangle$ and $|\bar{1}\sigma\rangle$ states

represented by the anti-nodal points. For $n = 2$ and the topological gap opened ($\mathcal{P}_\perp \neq 0$), the eigenvalue $\lambda_{\mathbf{k}\sigma}^{(-)}$ corresponds to the lower energy band which is fully filled and separated by a band gap from the empty $\lambda_{\mathbf{k}\sigma}^{(+)}$ band. To determine the Chern number we focus on the fully filled $\lambda_{\mathbf{k}\sigma}^{(-)}$ band.

The Chern number is defined as the integral of the Berry curvature over the Brillouin zone. In our case of system, which can be described by the block diagonal Hamiltonian given in Eq. (B1), the Chern number can be determined for each of the blocks representing different spin configurations. Namely,

$$C_\sigma = \frac{1}{2\pi} \iint_{\Omega_{\text{BZ}}} [\nabla_{\mathbf{k}} \times \mathbf{A}_\sigma(\mathbf{k})] \cdot d^2k \quad (\text{B8})$$

where

$$\nabla_{\mathbf{k}} = \left(\frac{\partial}{\partial k_x}, \frac{\partial}{\partial k_y} \right), \quad \mathbf{A}_\sigma(\mathbf{k}) = i \langle u_{\mathbf{k}\sigma}^{(-)} | \nabla_{\mathbf{k}} | u_{\mathbf{k}\sigma}^{(-)} \rangle. \quad (\text{B9})$$

We can equivalently calculate the Chern number by using

the following equation

$$C_\sigma = -\frac{1}{\pi} \oint_{C_F} \mathbf{A}_\sigma(\mathbf{k}) \cdot d\mathbf{k} = \frac{1}{2\pi} \oint_{C_F} \nabla_{\mathbf{k}} \phi_{\mathbf{k}\sigma} \cdot d\mathbf{k}, \quad (\text{B10})$$

where the curve C_F over which the integration is carried out corresponds to equal contribution of the $|2\sigma\rangle$ and $|1\bar{\sigma}\rangle$ states in the resultant eigenstate $|u_{\mathbf{k}\sigma}^{(-)}\rangle$. Such a situation appears at the equator of the Bloch sphere, where we are equally distant from the antipodal points, since from Eq. (B5) we have

$$\left| e^{i(\phi_{\mathbf{k}\sigma} - \pi)} \sin \frac{\theta_{\mathbf{k}\sigma}}{2} \right| = \frac{1}{\sqrt{2}}, \quad \left| \cos \frac{\theta_{\mathbf{k}\sigma}}{2} \right| = \frac{1}{\sqrt{2}}, \quad (\text{B11})$$

which implies that

$$\theta_{\mathbf{k}\sigma} = \frac{\pi}{2}. \quad (\text{B12})$$

Equivalently, from the last expression and by using Eqs. (B4) and (B6), one can explicitly determine the condition for the C_F curve in the \mathbf{k} -space

$$\epsilon_{\mathbf{k}\sigma}^{11} = \epsilon_{\mathbf{k}\sigma}^{22} \quad (\text{B13})$$

From Eq. (B10) one can see that the Chern number can be determined by calculating the winding of the complex phase of the hybridization term ($\phi_{\mathbf{k}\sigma}$) around the curve determined by (B13)

-
- [1] B. A. Foutty, C. R. Kometter, T. Devakul, A. P. Reddy, K. Watanabe, T. Taniguchi, L. Fu, and B. E. Feldman, Mapping twist-tuned multiband topology in bilayer WSe_2 , *Science* **384**, 343 (2024).
 - [2] F. Xu, Z. Sun, T. Jia, C. Liu, C. Xu, C. Li, Y. Gu, K. Watanabe, T. Taniguchi, B. Tong, J. Jia, Z. Shi, S. Jiang, Y. Zhang, X. Liu, and T. Li, Observation of integer and fractional quantum anomalous hall effects in twisted bilayer MoTe_2 , *Phys. Rev. X* **13**, 031037 (2023).
 - [3] F. Zhang, N. Morales-Durán, Y. Li, W. Yao, J.-J. Su, Y.-C. Lin, C. Dong, X. Liu, F.-X. R. Chen, H. Kim, K. Watanabe, T. Taniguchi, X. Li, J. A. Robinson, A. H. Macdonald, and C.-K. Shih, Experimental signature of layer skyrmions and implications for band topology in twisted WSe_2 bilayers (2025), arXiv:2406.20036 [cond-mat.mes-hall].
 - [4] Y. Xia, Z. Han, K. Watanabe, T. Taniguchi, J. Shan, and K. F. Mak, Unconventional superconductivity in twisted bilayer WSe_2 (2024), arXiv:2405.14784 [cond-mat.mes-hall].
 - [5] A. Jindal, A. Saha, Z. Li, T. Taniguchi, K. Watanabe, J. C. Hone, T. Birol, R. M. Fernandes, C. R. Dean, A. N. Pasupathy, and D. A. Rhodes, Coupled ferroelectricity and superconductivity in bilayer Td-MoTe_2 , *Nature* **613**, 48–52 (2023).
 - [6] Y. Tang, L. Li, T. Li, Y. Xu, S. Liu, K. Barmak, K. Watanabe, T. Taniguchi, A. H. Macdonald, J. Shan, and K. F. Mak, Simulation of Hubbard model physics in WSe_2/WS_2 moiré superlattices, *Nature* **579**, 353 (2020).
 - [7] Z. Han, Y. Xia, Z. Xia, W. Zhao, Y. Zhang, K. Watanabe, T. Taniguchi, J. Shan, and K. F. Mak, Evidence of topological Kondo insulating state in $\text{MoTe}_2/\text{WSe}_2$ moiré bilayers (2025), arXiv:2507.03287 [cond-mat.mes-hall].
 - [8] W. Zhao, B. Shen, Z. Tao, Z. Han, K. Kang, K. Watanabe, T. Taniguchi, K. F. Mak, and J. Shan, Gate-tunable heavy fermions in a moiré Kondo lattice, *Nature* **616**, 61–65 (2023).
 - [9] E. C. Regan, D. Wang, C. Jin, M. I. Bakti Utama, B. Gao, X. Wei, S. Zhao, W. Zhao, Z. Zhang, K. Yumigeta, M. Blei, J. D. Carlström, K. Watanabe, T. Taniguchi, S. Tongay, M. Crommie, A. Zettl, and F. Wang, Mott and generalized wigner crystal states in WSe_2/WS_2 moiré superlattices, *Nature* **579**, 359–363 (2020).
 - [10] H. Li, Z. Xiang, A. P. Reddy, T. Devakul, R. Sailus, R. Banerjee, T. Taniguchi, K. Watanabe, S. Tongay, A. Zettl, L. Fu, M. F. Crommie, and F. Wang, Wigner Molecular Crystals from Multi-electron Moiré Artificial Atoms (2023), arXiv:2312.07607 [cond-mat.mes-hall].
 - [11] X. Xu, W. Yao, D. Xiao, and T. F. Heinz, Spin and pseudospins in layered transition metal dichalcogenides, *Nature Physics* **10**, 343 (2014).
 - [12] K. F. Mak, D. Xiao, and J. Shan, Light-valley interactions in 2D semiconductors, *Nature Photonics* **12**, 451 (2018).

- [13] D. Xiao, G.-B. Liu, W. Feng, X. Xu, and W. Yao, Coupled Spin and Valley Physics in Monolayers of MoS_2 and Other Group-VI Dichalcogenides, *Phys. Rev. Lett.* **108**, 196802 (2012).
- [14] L. Rademaker, Spin-orbit coupling in transition metal dichalcogenide heterobilayer flat bands, *Phys. Rev. B* **105**, 195428 (2022).
- [15] T. Devakul and L. Fu, Quantum Anomalous Hall Effect from Inverted Charge Transfer Gap, *Phys. Rev. X* **12**, 021031 (2022).
- [16] T. Li, S. Jiang, B. Shen, Y. Zhang, L. Li, Z. Tao, T. Devakul, K. Watanabe, T. Taniguchi, L. Fu, J. Shan, and K. F. Mak, Quantum anomalous Hall effect from intertwined moiré bands, *Nature* **600**, 641 (2021).
- [17] W. Zhao, K. Kang, L. Li, C. Tschirhart, E. Redekop, K. Watanabe, T. Taniguchi, A. Young, J. Shan, and K. F. Mak, Realization of the Haldane Chern insulator in a moiré lattice (2022), arXiv:2207.02312 [cond-mat.mes-hall].
- [18] Y. Zhang, T. Devakul, and L. Fu, Spin-textured Chern bands in AB-stacked transition metal dichalcogenide bilayers, *Proceedings of the National Academy of Sciences* **118**, e2112673118 (2021).
- [19] H. Pan, M. Xie, F. Wu, and S. Das Sarma, Topological Phases in AB-Stacked $\text{MoTe}_2/\text{WSe}_2$: Z_2 Topological Insulators, Chern insulators, and Topological Charge Density Waves, *Phys. Rev. Lett.* **129**, 056804 (2022).
- [20] Y.-M. Xie, C.-P. Zhang, J.-X. Hu, K. F. Mak, and K. T. Law, Valley-Polarized Quantum Anomalous Hall State in moiré $\text{MoTe}_2/\text{WSe}_2$ heterobilayers, *Phys. Rev. Lett.* **128**, 026402 (2022).
- [21] T. Devakul and L. Fu, Quantum anomalous hall effect from inverted charge transfer gap, *Phys. Rev. X* **12**, 021031 (2022).
- [22] Y.-W. Chang and Y.-C. Chang, Quantum anomalous hall effect and electric-field-induced topological phase transition in AB-stacked $\text{MoTe}_2/\text{WSe}_2$ moiré heterobilayers, *Phys. Rev. B* **106**, 245412 (2022).
- [23] P. Saha, L. Rademaker, and M. Zegrodnik, Interplay between topology and electron-electron interactions in the moiré $\text{MoTe}_2/\text{WSe}_2$ heterobilayer, *Phys. Rev. B* **112**, 045147 (2025).
- [24] Y.-M. Xie, C.-P. Zhang, and K. T. Law, Topological $p_x + ip_y$ intervalley coherent state in moiré $\text{MoTe}_2/\text{WSe}_2$ heterobilayers, *Phys. Rev. B* **110**, 045115 (2024).
- [25] Y.-M. Xie, C.-P. Zhang, J.-X. Hu, K. F. Mak, and K. T. Law, Valley-Polarized Quantum Anomalous Hall state in Moiré $\text{MoTe}_2/\text{WSe}_2$ heterobilayers, *Phys. Rev. Lett.* **128**, 026402 (2022).
- [26] D. Guerci, J. Wang, J. Zang, J. Cano, J. H. Pixley, and A. Millis, Chiral kondo lattice in doped $\text{MoTe}_2/\text{WSe}_2$ bilayers, *Science Advances* **9**, eade7701 (2023).
- [27] D. Guerci, K. P. Lucht, V. Crépel, J. Cano, J. H. Pixley, and A. Millis, Topological Kondo semimetal and insulator in AB-stacked heterobilayer transition metal dichalcogenides, *Phys. Rev. B* **110**, 165128 (2024).
- [28] P. Froese, T. Neupert, and G. Wagner, Topological excitons in moiré $\text{MoTe}_2/\text{WSe}_2$ heterobilayers, *Phys. Rev. Res.* **7**, 023047 (2025).
- [29] Z. Dong and Y.-H. Zhang, Excitonic Chern insulator and kinetic ferromagnetism in a $\text{MoTe}_2/\text{WSe}_2$ moiré bilayer, *Phys. Rev. B* **107**, L081101 (2023).
- [30] C. L. Kane and E. J. Mele, Z_2 Topological Order and the Quantum Spin Hall Effect, *Phys. Rev. Lett.* **95**, 146802 (2005).
- [31] F. D. M. Haldane, Model for a quantum hall effect without landau levels: Condensed-matter realization of the "parity anomaly", *Phys. Rev. Lett.* **61**, 2015 (1988).
- [32] M. Zegrodnik, Quantum Valley Hall insulator in $\text{MoTe}_2/\text{WSe}_2$ heterobilayer [data set]. zenodo. <https://doi.org/10.5281/zenodo.17789146>, 10.5281/zenodo.17789146 (2025).